ACS APPLIED MATERIALS & INTERFACES

www.acsami.org

Forum Article

4D Printing of Bioinspired Absorbable Left Atrial Appendage Occluders: A Proof-of-Concept Study

Cheng Lin, Liwu Liu,* Yanju Liu, and Jinsong Leng*

Cite This: *ACS Appl. Mater. Interfaces* 2021, 13, 12668−12678

Read Online

ACCESS | Metrics & More | Article Recommendations | Supporting Information

ABSTRACT: The significant mismatch of mechanical properties between the implanted medical device and biological tissue is prone to cause wear and even perforation. In addition, the limited biocompatibility and nondegradability of commercial Nitinol-based occlusion devices can easily lead to other serious complications, such as allergy and corrosion. The present study aims to develop a 4D printed patient-specific absorbable left atrial appendage occluder (LAAO) that can match the deformation of left atrial appendage (LAA) tissue to reduce complications. The desirable bioinspired network is explored by iterative optimization to mimic the stress−strain curve of LAA tissue and LAAOs are designed based on the optimal network. In vitro degradation tests are carried out to evaluate the effects of degradation on mechanical properties. In addition, 48 weeks of long-term subcutaneous implantation of the occluder shows favorable biocompatibility, and the 20-cycle compression test demonstrates outstanding durability of LAAO. Besides, a rapid, complete, and remote-controlled 4D transformation process of LAAO is achieved under the trigger of the magnetic field. The deployment of the LAAO in an isolated swine heart initially exhibits its feasibility for transcatheter LAA occlusion. To the best of our knowledge, this is the first demonstration of the 4D printed LAA occlusion device. It is worth noting that the bioinspired design concept is not only applicable to occlusion devices, but also to many other implantable medical devices, which is conducive to reducing complications, and a broad range of appealing application prospects can be foreseen.

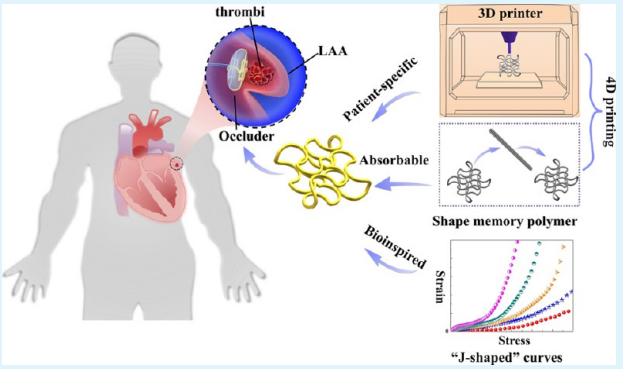

KEYWORDS: *4D printing, shape memory polymers, left atrial appendage occluders, biodegradable occluders, bioinspired structures, tailored mechanical properties*

1. INTRODUCTION

3D printing is increasingly being used across a wide spectrum of biomedical fields due to the accuracy and effectiveness of manufacturing complex structures, such as drug delivery systems, various implantable scaffolds, organ regenerations, etc.[1−3] Shape memory polymer (SMP) is a type of stimulus-responsive material that is able to recover from a deformed temporary shape to the initial shape upon external activations (e.g., heat, light, magnetic field, etc.).[4−6] SMP has aroused widespread research interest in biomedicine because of the excellent biocompatibility, biodegradability, and great potential for minimally invasive therapy.[7−11] The combination of active materials (e.g., SMP) and 3D printing, namely, 4D printing, enables the structural reconfiguration of 3D printed components over time. When introduced to medical devices, 4D printing endows them with customized geometries, as well as dynamic and transformable capabilities.[12−14]

Atrial fibrillation (AF) is the most common cardiac arrhythmia; it increases the risk of stroke 5-fold and is associated with approximately 15−20% of ischemic stroke.[15,16] For nonvalvular AF patients, over 90% of atrial thrombi originate from the left atrial appendage (LAA),[17] which is a small pouch protruding from the left atrium with a complex internal structure (Figure 1). If the thrombus formed in LAA escapes and blocks the blood vessels supplying the brain, it will lead to a life-threatening stroke.[18] Long-term use of oral anticoagulants (OACs) can effectively reduce the risk of stroke associated with AF.[19] However, due to the serious side effects of OACs, such as endless monitoring, narrow treatment range, multiple food/drug interactions, and even fatal bleeding, approximately 40% of high-risk stroke patients are not eligible for OAC anticoagulation therapy.[16,20] Hence, transcatheter closure of LAA is considered as an improved nonpharmacological alternative to OACs to prevent stroke from the source, especially suitable for OAC-ineligible AF patients.[21] The earliest left atrial appendage

Special Issue: Novel Stimuli-Responsive Materials for 3D Printing

Received: September 24, 2020
Accepted: December 22, 2020
Published: January 5, 2021

https://dx.doi.org/10.1021/acsami.0c17192
ACS Appl. Mater. Interfaces 2021, 13, 12668−12678

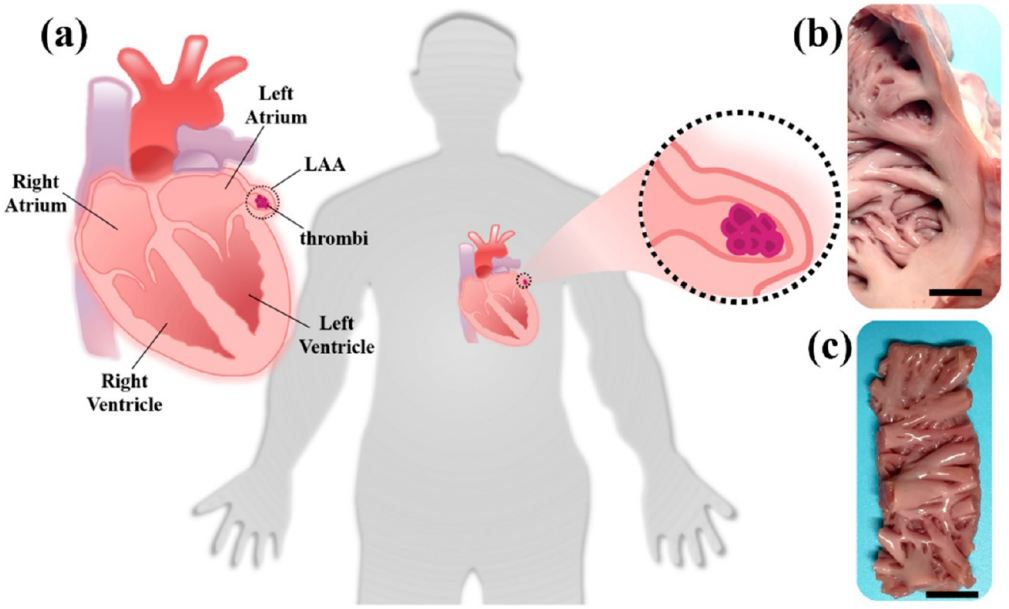

Figure 1. (a) Schematic of LAA with thrombi. (b) LAA tissue of swine. (c) LAA tissue for tensile testing. Scale bar = 10 mm.

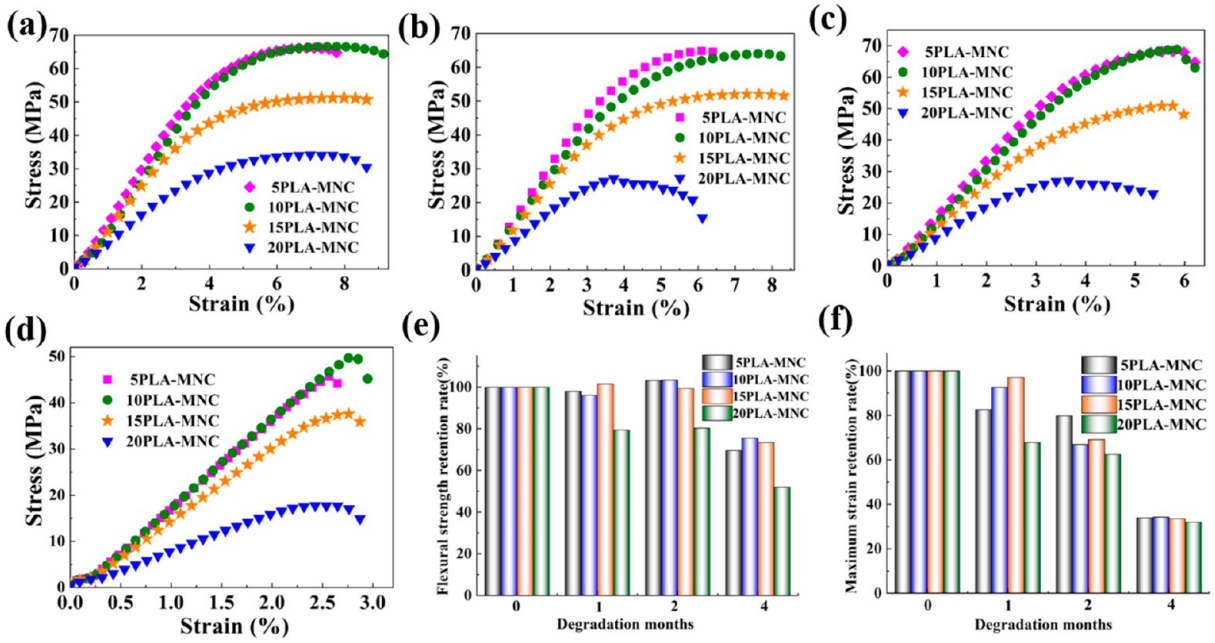

Figure 2. Three-point bending tests of PLA-MNCs degraded for (a) 0 months, (b) 1 month, (c) 2 months, and (d) 4 months. (e) Flexural strength retention rate (the ratio of the flexural strength of the degraded specimen to that of the nondegraded specimen) of PLA-MNCs at different degradation months. (f) Maximum strain retention rate (the ratio of the fracture strain of the degraded specimen to that of the nondegraded specimen) of PLA-MNCs at different degradation months.

occluder (LAAO) was PLAATO (Appriva Medical, USA), which was first implanted in the human body in 2001.[22] Currently, LAAOs for clinical applications include the Watchman device (Boston Scientific, Marlborough, USA), Amplatzer Amulet Device (Abbott, Abbott Park, USA), LAmbre device (Lifetech Scientific, Shenzhen, China), etc. Although these clinically used Nitinol-based occlusion devices are effective in isolating LAA, their limited biocompatibility and nondegradability can easily result in complications such as allergy and corrosion.[23,24] More seriously, the significant mismatch of the mechanical properties between the metal device and the surrounding tissue will cause severe tissue wear and even perforation.[25] Therefore, it is of great significance to develop biocompatible and absorbable LAAOs that can match the deformation of biological tissues.

Ideally, the implanted LAA occluder provides a temporary platform for the closure of the LAA, allowing the surrounding tissue to grow into the occluder. After endothelialization, a "self-closing" will be achieved; thus, the occluder is no longer needed. An absorbable transcatheter patch made of polyurethane foam was developed to occlude different heart defects including LAA.[26,27] However, the patch had to be inflated with a balloon

https://dx.doi.org/10.1021/acsami.0c17192
ACS Appl. Mater. Interfaces 2021, 13, 12668−12678

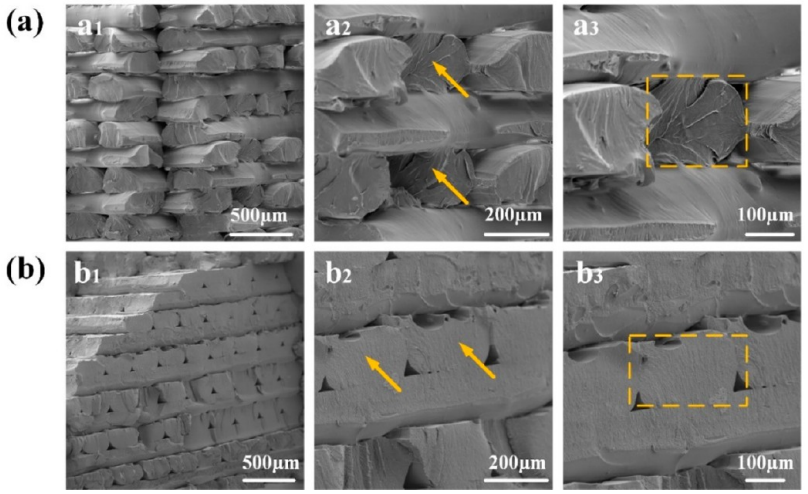

Figure 3. Fracture surface morphologies of 10PLA-MNC three-point bending specimens (a) before degradation and (b) after degradation for 4 months.

and secured with surgical adhesive to prevent migration, which increased the complexity of the procedure. No other reports on absorbable LAAOs have been found, indicating that the investigation and exploration of absorbable LAAOs are far from enough.

The purpose of the present study was to develop a 4D printed bioinspired absorbable LAAO with tailored mechanical properties, enabling it to provide mechanical support for LAA sufficiently and deform cooperatively with LAA tissue. Inspired by collagen fibrils, network materials with wavy microstructure were developed and employed to explore the desirable LAAO structure, because the materials were able to mimic nonlinear "J-shaped" stress−strain curves of biological tissues and exhibit synergistic deformation with tissues.[28−32,37] Iterative optimization was carried out through finite element analysis (FEA) to determine the optimal bioinspired structure, and two types of LAAOs were devised based on the optimal structure. LAAOs were fabricated by 4D printing using shape memory PLA-based magnetic nanocomposites (PLA-MNCs), in which magnetic nanoparticles were added to ensure the self-heating and remote-controlled 4D transformation of LAAOs. The mechanical properties of the shape memory PLA-MNCs during degradation were investigated and the morphologies were examined. In addition, long-term in vivo biocompatibility, compression test, shape memory performance, and the in vitro feasibility demonstration of transcatheter LAA occlusion of the bioinspired LAAO were systematically investigated.

2. RESULTS AND DISCUSSION

2.1. Effects of Degradation on Mechanical Properties.

To investigate the flexural properties of shape memory PLA-MNCs, three-point bending tests were performed. The flexural strength σ_f and maximum strain ε of the midspan outer surface were calculated using the following formulas:[33]

$$\sigma_f = \frac{3PL_s}{2wt^2} \quad (1)$$

$$\varepsilon = \frac{6\delta t}{L_s^2} \quad (2)$$

where P, L_s, w, t, and δ represent the maximum load, span distance, specimen width, specimen thickness, and midspan displacement, respectively. Figure 2a displays the stress−strain behaviors of PLA-MNCs under flexural loading conditions. The shape memory PLA-MNCs with different contents of Fe_3O_4 magnetic nanoparticles (5, 10, 15, and 20 wt %) were abbreviated as 5PLA-MNC, 10PLA-MNC, 15PLA-MNC, and 20PLA-MNC. The flexural strengths of 5PLA-MNC and 10PLA-MNC were about 68 MPa, while the flexural strengths of 15PLA-MNC and 20PLA-MNC were decreased due to the agglomeration of nanoparticles, and the flexural strength of 20PLA-MNC was approximately 34 MPa.

Absorbable medical devices will undergo degradation after implantation; thus, it is necessary to investigate the effects of degradation on mechanical properties.[34] Figure 2b−d shows the stress−strain behaviors of PLA-MNCs after different degradation times under flexural loading conditions. In general, the flexural strength and strain at break of PLA-MNCs decreased with the increase of degradation time (Figure 2e,f), which was attributed to the scission of the PLA-MNCs backbone.[35] After 2 months of degradation, the flexural strength of MNCs was maintained at 96.5% on average, and the strain at break of PLA-MNCs was maintained at 69.5% on average. After the fourth degradation month (Figure 2d), the flexural strengths of 5PLA-MNC, 10PLA-MNC, 15PLA-MNC, and 20PLA-MNC were approximately 50, 45, 38, and 18 MPa, respectively. The strain at break of PLA-MNCs decreased to approximately 33% on average (Figure 2f). For 10PLA-MNC, the flexural strength retention rate and the maximum strain retention rate were 75.5% and 34.0%, respectively. In addition, the tensile tests of 10PLA-MNC specimens before and after degradation showed similar results to the three-point bending tests, that is, the strength and strain at break decreased due to degradation (Figures S1−S2).

Figure 3 shows the fracture surface morphologies of the PLA-MNCs flexural specimens. The overall surface morphologies showed the shape of a brick wall, and the printing process of layer-by-layer deposition can be seen (Figure 3a_1,b_1). The formation of massive crazing is a way to toughen polymers,[36] and crazes on the surface of the undegraded specimen can be observed in Figure 3a (indicated by the yellow arrows and square). After degradation for 4 months (Figure 3b), the fracture surface morphologies of the degraded specimen became much smoother, and the decrease of crazes meant reduced toughness. This phenomenon was in agreement with the three-point

https://dx.doi.org/10.1021/acsami.0c17192
ACS Appl. Mater. Interfaces 2021, 13, 12668−12678

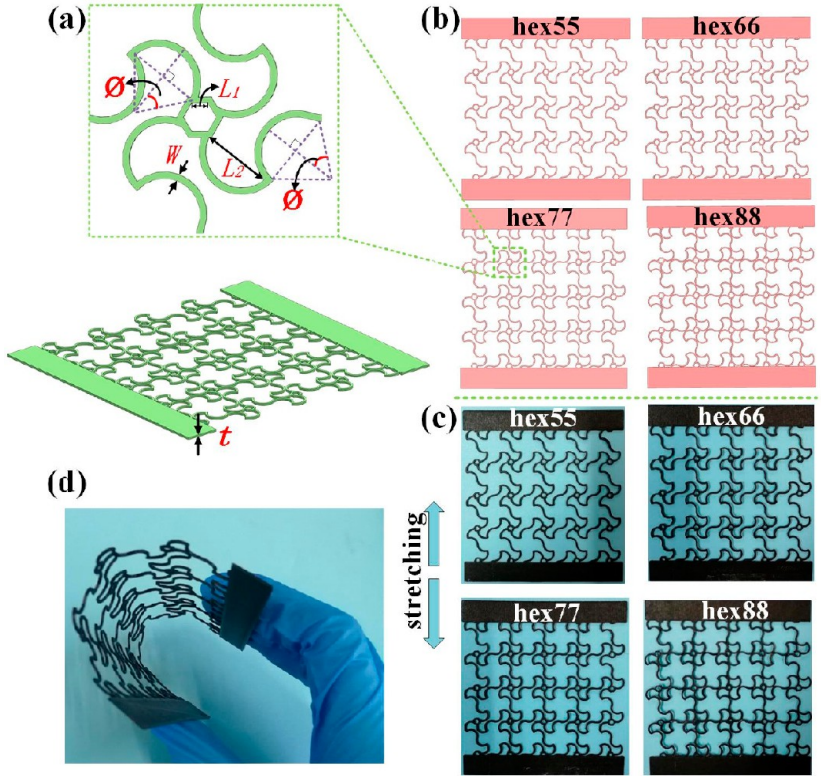

Figure 4. Bioinspired 2D networks. (a) Geometric parameters. (b) 3D models of four candidate bioinspired 2D networks. (c) 3D printed four candidate bioinspired 2D networks. (d) Flexibility demonstration of the 2D network.

bending test results in Figure 2f, in which strain at break was decreased visibly after 4 months of degradation. Similar results can be obtained from the fracture surface morphologies of the tensile specimens (Figure S4).

2.2. Structure Exploration of Bioinspired LAAOs. The network material with wavy filament microstructure is able to exhibit nonlinear "J-shaped" stress−strain behavior similar to skin and blood vessels, and can accurately reproduce the mechanical properties of the biological tissues, showing attractive application prospects in wearable electronics and tissue engineering.[30] The "J-shaped" stress−strain response is characterized by a low modulus response under small strains, followed by a transition zone in which the modulus slowly rises, and finally a sharp rise under large strains. Therefore, the material with "J-shaped" stress−strain behavior can conform to the deformation of biological tissue under small strains, which can greatly reduce the tissue wear and even perforation caused by the huge difference in mechanical properties between the implant and biological tissue; under large strains, the high elastic modulus of the material endows it with a natural "strain limiting" ability, which can prevent excessive deformation of tissue and the implanted device, thus reducing the risk of mechanically induced device failure and further protecting the tissue.[28−32]

The repeating unit of the bioinspired network is composed of a hexagonal central node and four ligaments, each of which consists of two identical arcs (Figure 4a). The repeating units are arranged in four in the stretching direction and five in the width direction to form a 2D bioinspired network. The dimensionless geometric parameters ($2Ø$, L_2/L_1, W/L_1, t/L_1) of the bioinspired network determine its macroconfiguration and mechanical performance. $2Ø$ is the arc angle, L_2 is the arc span, W is the width, L_1 is the length of the hexagon node, and t is the thickness of the network. The diversity of geometric parameters allows the mechanical properties of the bioinspired network to be widely adjustable, which provides the possibility for the customization of mechanical properties.

Iterative optimization was performed through FEA (ABAQUS software package) to determine the necessary parameters of the bioinspired network to control the "J-shaped" stress−strain behavior. The specific process was as follows. A bioinspired 2D network model library was built based on various design parameters. The stress−strain curves of the 2D networks with different parameters were calculated by FEA and compared with the stress−strain behavior of LAA tissue. Under the guidance of searching for a bioinspired 2D network similar to the deformation behavior of LAA (to deform cooperatively with LAA) but with higher stiffness (to provide sufficient support for LAA), the scope of the bioinspired 2D network model library was gradually reduced. Finally, four bioinspired 2D networks were selected as the candidate structures of LAAOs (Figure 4b), where the deterministic parameters of networks were L_2/L_1 = 4.2, W/L_1 = 0.4, t/L_1 = 0.53, and Ø = 55°/66°/77°/88°. Figure 4c is the visual demonstration of the four candidate 2D networks manufactured by fused deposition modeling (FDM) 3D printing, and the flexibility of the printed network is shown in Figure 4d. In addition, the stress and displacement distributions of the 2D hex88 network predicted by FEA during the uniaxial tensile process are shown in Figure 5a,b, and the experimental deformation process is shown in Figure 5c. It can be seen that the tensile deformation behavior obtained by experiments and simulations showed good consistency. The entire stretching process of hex88 was recorded and provided as Movie S1. The deformation sequences of three other 2D networks with different ligament curvatures (hex77, hex66, and hex55) are depicted in Figures S5, S6, and S7.

https://dx.doi.org/10.1021/acsami.0c17192
ACS Appl. Mater. Interfaces 2021, 13, 12668−12678

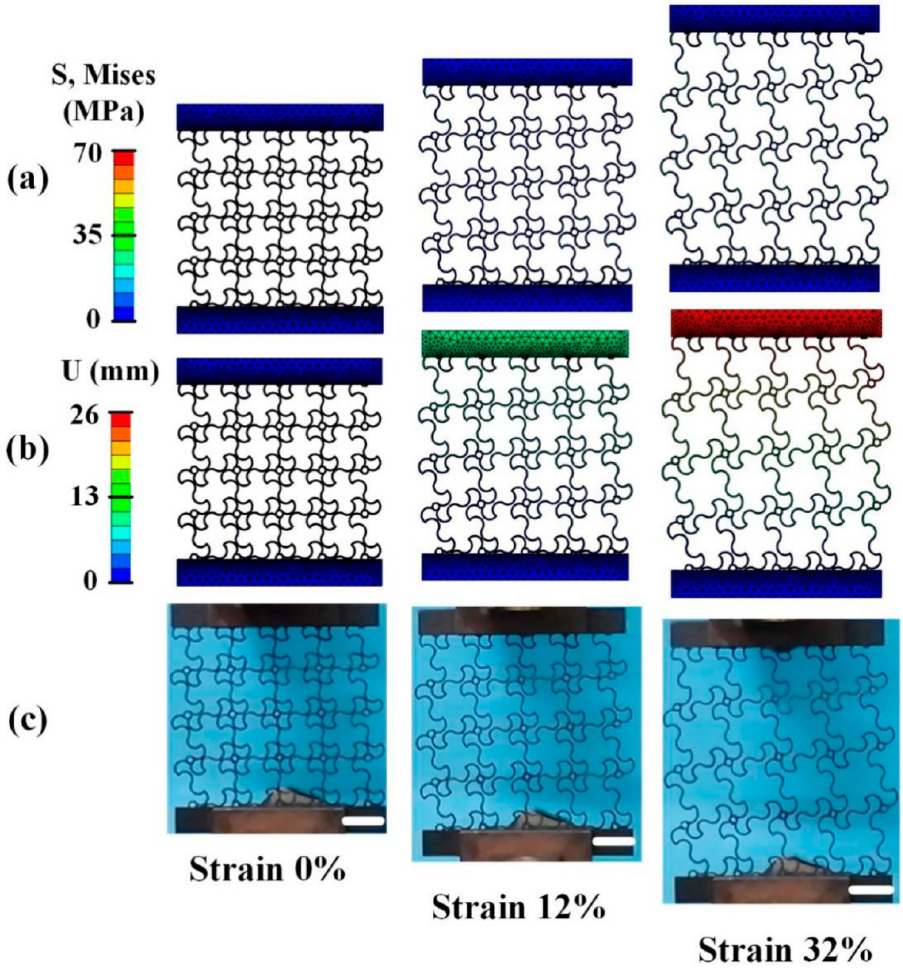

Figure 5. Uniaxial tensile deformation sequences of 2D hex88 network under different strains. Deformations predicted by FEA (a) stress distribution and (b) displacement distribution. (c) Experimental deformation process. Scale bar = 20 mm.

Figure 6a shows the stress−strain curves of four printed 2D networks (hex55, hex66, hex77, and hex88) and LAA tissue under tensile load. Like many other biological materials, such as blood vessels and skin,[32,37] the LAA tissue exhibited a "J-shaped" stress−strain response, and the four printed bioinspired 2D networks showed similar responses. The response of bioinspired networks to uniaxial tensile load was mainly expressed in three stages, during which the ligaments became flat gradually. The representative repeating units of the three stages are shown in the insets of Figure 6a. At the initial stage, the deformation was dominated by bending, leading to a very low modulus. Then, with further stretching (second stage), the ligaments rotated and were parallel to the stretching direction. The nodes also rotated with the deformation of the ligaments. In the second stage, the deformation mode of the network gradually changed from bending dominated to stretching dominated, and the modulus exhibited a slow increase. In the final stage, the nodes and flat ligaments parallel to the stretching direction were directly stretched without rotational deformation as a buffer, resulting in a sharp increase in modulus. The details of the three stages can be observed through Movie S1. As shown in Figure 6a, the stress−strain response of the hex88 network was the closest to LAA, with a modulus slightly higher than that of the LAA tissue, satisfying the requirements of providing sufficient mechanical support for LAA while matching LAA deformation. Therefore, hex88 was selected as the optimal bioinspired structure.

Based on the bioinspired hex88 network, two kinds of LAAOs (single-layer LAAO and double-layer LAAO) were developed. Figure 6b,c shows the 3D models of single-layer and double-layer LAAOs. 10PLA-MNC filaments were used to manufacture LAAOs through 4D printing technology due to the superior mechanical properties. To improve the occlusion capability,[38−41] blocking membranes prepared by electrospinning were sewn to the printed LAAOs with biodegradable PGA sutures. As displayed in Figure 6d, the uniform nanofiber distribution of the electrospun membrane can be observed with a scanning electron microscope (SEM). Figure 6e,f displays the printed single-layer and double-layer LAAOs, while Figure 6g,h shows the visual demonstrations of LAAOs with blocking membranes.

The compressive behaviors of LAAOs were investigated, as shown in Figure 6i. The single-layer LAAO can withstand a maximum compression load of approximately 4.3 N. The double-layer LAAO showed a more flexible response and its deflection was much higher than the single-layer LAAO under the same load. Interestingly, the compression behavior of the double-layer LAAO also exhibited a bioinspired "J-shaped" curve, which was conducive to conforming to the deformation of LAA tissue under small strains and preventing device damage caused by excessive deformation under large strains. In addition, the durability of the double-layer LAAO was remarkable. It remained intact even after 20 compression cycle tests with a

https://dx.doi.org/10.1021/acsami.0c17192
ACS Appl. Mater. Interfaces 2021, 13, 12668−12678

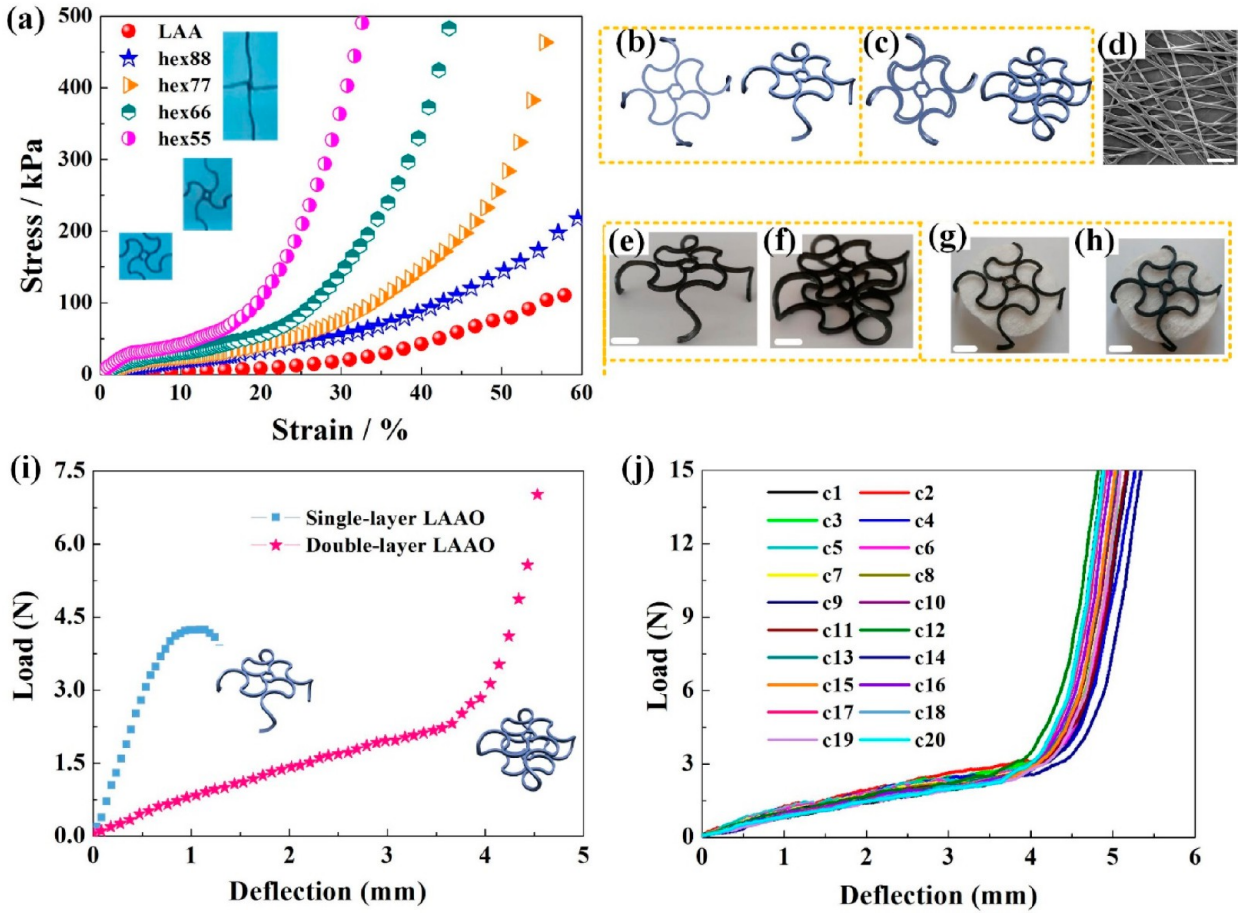

Figure 6. (a) Stress−strain curves of four printed candidate 2D networks (hex55, hex66, hex77, and hex88) and LAA tissue under tensile load. 3D models of (b) single-layer and (c) double-layer LAAOs. (d) SEM image of the electrospinning blocking membrane. Scale bar = 50 μm. Printed (e) single-layer and (f) double-layer LAAOs. Visual demonstration of (g) single-layer and (h) double-layer LAAOs with blocking membranes. (e−h) Scale bar = 5 mm. (i) Compressive behaviors of single-layer and double-layer LAAOs. (j) 20-cycle (c1-c20) compression test of double-layer LAAO.

maximum load of 15 N (Figure 6j). More importantly, the load-deflection curves showed no significant difference between the first and the 20th cycles, implying the double-layer LAAO maintained its mechanical properties throughout the cycle tests.

2.3. Biocompatibility Evaluation. To evaluate the in vivo biocompatibility, sterilized 10PLA-MNC occluders were subcutaneously implanted in male Sprague−Dawley mice.[47,48] Long time observation of tissue responses after implantation can better examine the biocompatibility, thus occluders were collected after 48 weeks of implantation. Figure 7a−c shows the hematoxylin-eosin (H&E) stained images of occluders and surrounding tissues. Mature fibrous tissues and blood vessels can be observed in Figure 7a, with a slight inflammatory response due to degradation and fragmentation of the implanted bioabsorbable occluder.[42] Denser connective tissues can be seen in Figure 7b, and the black part in the upper left corner was the occluder.[43] Figure 7c is a tissue section with longitudinally cut and evenly distributed muscle fibers at the edge of the implanted occluder. The major organs, including the heart, liver, spleen, lung, and kidney, were harvested to further investigate the biocompatibility,[49] and the results manifested that no significant histopathological damage or abnormality was found in the major organs (Figure 7d).

2.4. 4D Transformation of LAAOs and Feasibility Demonstration of Transcatheter LAA Closure. The heat-induced 4D transformation processes of single-layer LAAO and double-layer LAAO are displayed in Figure 8. The 4D printed LAAOs were programmed to straight temporary shapes with small cross-section areas to facilitate interventional delivery and implantation (Figure 8a1,b1). Dynamic, rapid, and complete 4D transformation processes of the two LAAOs were exhibited (Figure 8a1−a5, Figure 8b1−b5), demonstrating excellent shape memory properties. Figure 8a6,b6 shows side views of the final state of the single-layer and double-layer LAAOs after 4D transformation, almost maintaining their original configurations. The recovery time of single-layer LAAO was slightly longer than that of double-layer LAAO, which might be due to the fact that the higher content of shape memory MNCs in double-layer LAAO endowed it with greater recovery force. In addition, the degree of freedom of the double-layer LAAO structure was lower than that of the single-layer LAAO, and the overall coordinated deformation of the double-layer LAAO structure led to less entropic strain energy loss during the 4D transformation. The video capturing the 4D transformation process of double-layer LAAO is provided as Movie S2.

The possibility of remotely controlled 4D transformation was verified by an alternating magnetic field. The magnetic field provides an efficient actuation method for remote control in biomedicine, especially in closed and inaccessible places, and its safety and effectiveness have been widely studied.[44−46] As shown in Figure 9, the straight temporary shape gradually recovered to the original bioinspired structure within half a

https://dx.doi.org/10.1021/acsami.0c17192
ACS Appl. Mater. Interfaces 2021, 13, 12668−12678

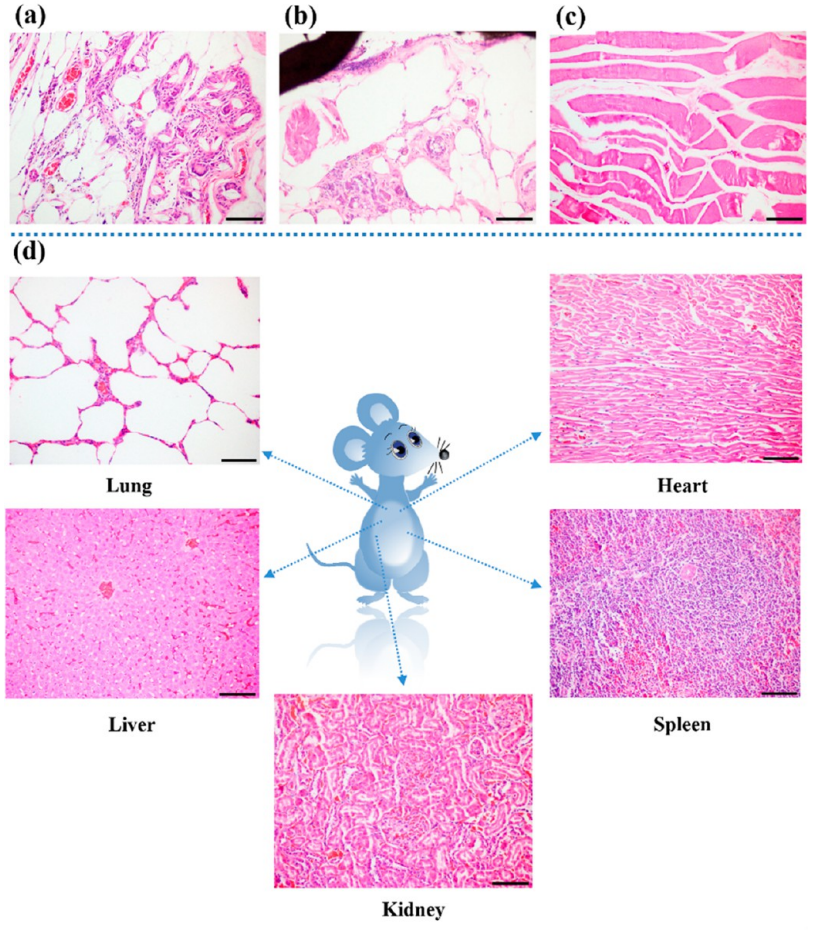

Figure 7. H&E staining of tissue sections 48 weeks after occluder implantation. (a–c) Occluder and its surrounding tissues. (d) Major organs of mice. Scale bar = 100 μm.

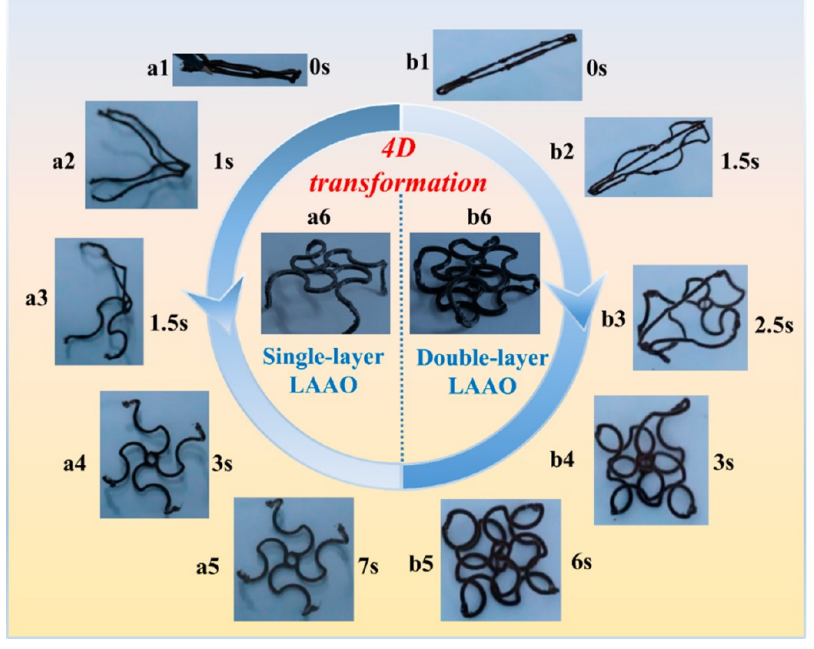

Figure 8. Heat-induced 4D transformation. Temporary shapes of (a1) single-layer LAAO and (b1) double-layer LAAO. 4D transformation processes of (a1–a5) single-layer LAAO and (b1–b5) double-layer LAAO. Side views of (a6) single-layer LAAO and (b6) double-layer LAAO after 4D transformation.

https://dx.doi.org/10.1021/acsami.0c17192
ACS Appl. Mater. Interfaces 2021, 13, 12668–12678

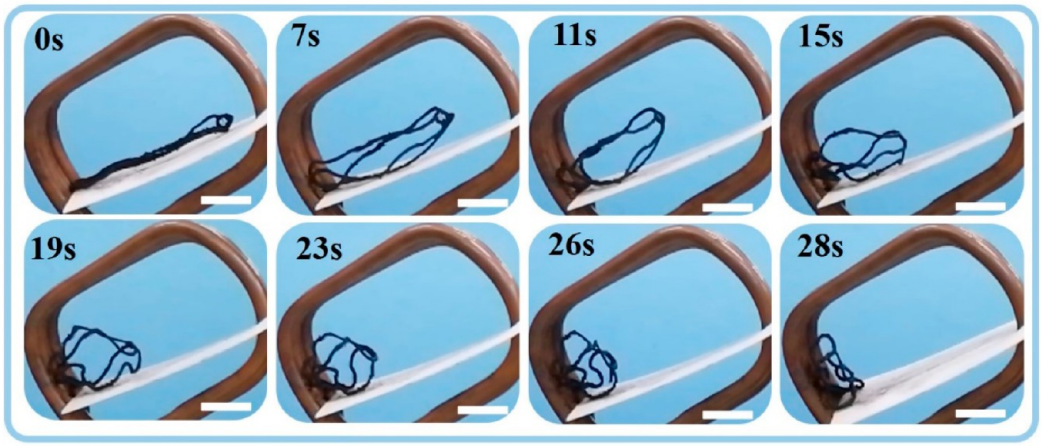

Figure 9. (a) Magnetism-induced 4D transformation process of double-layer LAAO. Scale bar = 10 mm.

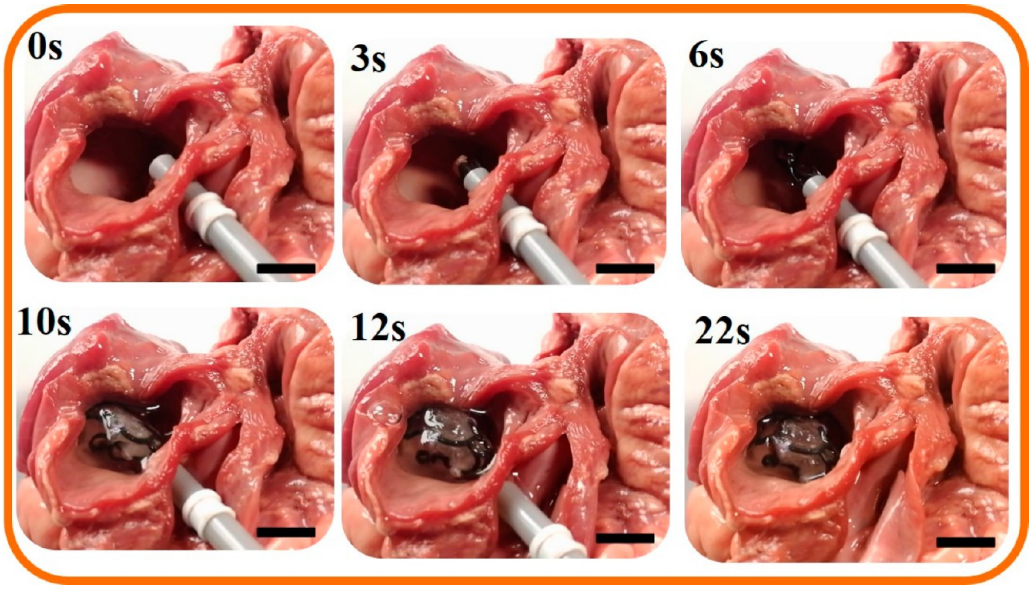

Figure 10. Feasibility demonstration of transcatheter LAA closure. Scale bar = 10 mm.

minute under the trigger of the magnetic field, showing the outstanding magnetic response performance of LAAO. Compared with the heat-induced recovery process, the magnetism-induced recovery process took longer. This might be because magnetic Fe_3O_4 particles acted as self-heaters during the recovery process, and the heat was transferred only within the LAAO structure, while the entire LAAO structure was immersed in water during the heat-induced recovery process, leading to larger heating area and much faster heat transfer speed.

The in vitro feasibility test of transcatheter LAA closure was performed using a 13 Fr. catheter to deliver the double-layer LAAO to the LAA of a freshly isolated swine heart. As displayed in Figure 10, the LAAO can be smoothly pushed out of the catheter, which indicated that minimally invasive implantation was accessible. LAAO was released close to the LAA orifice, and a complete LAAO deployment process can be observed, indicating the effectiveness of LAAO for LAA occlusion.

3. CONCLUSIONS

In summary, this work was dedicated to exploring bioinspired, patient-specific, and absorbable LAAOs. The introduction of the wavy ligaments improved the design freedom of the bioinspired structure and enabled customization of the mechanical properties to conform to LAA deformation and reduce tissue wear. 4D printing endowed LAAO with patient-specific geometry, and transformability between temporary and permanent configurations, thus ensuring perfect fit with LAA and enabling minimally invasive implantation. The results revealed that the mechanical properties of the developed double-layer LAAO were maintained even after 20 cyclic compression tests with a maximum load of 15 N, showing distinguished durability. Histological results at 48 weeks after implantation demonstrated that the occluder was biocompatible. The heat-induced 4D transformation process showed remarkable shape memory properties of LAAO. Besides, LAAO exhibited excellent magnetic response performance, which enabled a remote-controlled magnetism-induced 4D transformation. In addition, the deployment of the LAAO in isolated swine heart preliminarily verified its feasibility for transcatheter LAA closure.

Although the shape memory transition temperature of LAAO is a little high and needs further modification,[50,51] this work plays an irreplaceable role due to the lack of similar concepts and results in the professional literature. This work may contribute

https://dx.doi.org/10.1021/acsami.0c17192
ACS Appl. Mater. Interfaces 2021, 13, 12668−12678

to the development of state-of-the-art occlusion devices with patient-specific geometry, absorbability, and tailored mechanical properties to reduce tissue wear and other severe complications. More importantly, the bioinspired design approach for searching the desired device configuration is generic and flexible, and can be extended to many other implantable devices to obtain a wide range of appealing applications.

4. EXPERIMENTAL SECTION

4.1. Specimen Fabrication. PLA (Nature Works LLC. Ingeo 4032D, $M_w \approx 200{,}000$ g mol^{-1}) was completely dissolved in dichloromethane and Fe_3O_4 nanoparticles (Aladdin, Shanghai, China, 98%) were added with different mass fractions (5, 10, 15, and 20 wt %). Homogenized PLA-Fe_3O_4 suspension was obtained by continuous stirring for 24 h. After evaporating the solvent, the cured composites were cut into small pieces, and then the small pieces were extruded into filaments (diameter: ∼1.75 mm) through an extruder at 200 °C.

The printed models were created using NX 10.0 software and then converted to .stl files. The .gcode format files were generated by slicing software and the models were printed using FDM 3D printer (Allcct). The print orientation, speed, and nozzle temperature were set to 45°, 5 mm s^{-1}, and 195 °C, respectively. After printing, the post-treatment process of polishing LAAOs was carried out.

4.2. Mechanical Properties Characterization. Three-point bending tests of PLA-based shape memory MNCs were conducted following the ASTM D790. The tensile tests of the bioinspired networks and LAA tissue were performed with a loading rate of 1 mm min^{-1} and a preload of 0.2 N. The size of the LAA tissue for tensile tests was approximately 50 mm × 18 mm × 6.5 mm (Figure 1c). In addition, the compression tests of LAAOs were carried out at a loading rate of 1 mm min^{-1}. All specimens were prepared by FDM 3D printer and tested with Zwick 010 machine at room temperature.

4.3. In Vitro Degradation Test. In vitro degradation tests were performed by incubating the printed specimens in phosphate-buffered saline solution (PH = 7.4) at 37 °C. The specimens were removed periodically, washed with distilled water, and dried in a vacuum to prepare for testing. The solution was replaced every 7 days.

4.4. Electrospinning of Blocking Membranes. The polymer solution with a concentration of 8 wt % was prepared by dissolving PLA in dichloromethane and stirred for 24 h at 25 °C. The injection rate was 1.5 mL h^{-1} and the voltage was maintained at 15 kV. A flat sheet of aluminum foil 170 mm from the tip served as a collector.

4.5. Morphological Observation. The fractured specimens were collected after mechanical tests, and the surface morphologies of the fractured specimens perpendicular to the tensile direction were examined by SEM (VEGA3 TESCAN) with an accelerating voltage of 10 kV. The morphologies of the blocking membranes were also observed under the same accelerating voltage.

4.6. In Vivo Biocompatibility Evaluation. In vivo biocompatibility was conducted under the guidance approved by the Ethics Research Committee of the Harbin Institute of Technology. The occluders were sterilized and placed subcutaneously in male Sprague−Dawley mice. 48 weeks later, the occluders and major organs were collected from euthanized mice. Next, formalin-fixed paraffin-embedded tissue slices (5 μm) were stained by H&E staining kit and analyzed via light microscope (DP73, OLYMPUS, Japan).

4.7. Shape Memory Performance (4D Transformation) Characterization. The glass transition temperature (T_g) of the 10PLA-MNC was 62.7 °C.[52] The printed LAAO was first placed in a water bath at a temperature of T_g +10 °C for 10 min, and then programmed into a straight temporary shape. The LAAO with straight temporary shape was immediately cooled to room temperature and maintained for an additional 5 min to fix the configuration. The heat-induced 4D transformation process was carried out in the same hot water bath as the programming process, while the magnetism-induced 4D transformation process was performed in an alternating magnetic field (intensity: 4 kA m^{-1}).

4.8. In Vitro Feasibility Demonstration of Transcatheter LAA Closure. Freshly isolated swine hearts were used to evaluate the feasibility of the LAAO. To show the shape recovery of the double-layer LAAO more clearly, the cardiac tissue near the orifice of LAA was partially excised. After trans-septal puncture with a Brockenbrough needle,[53] the double-layer LAAO was delivered to the LAA using a 13 Fr. catheter (Starway Medical Technology, Inc.). Once the optimal position was identified, a small amount of hot physiological saline (T_g +10 °C) was injected from the other side of the catheter and the recovery of the occluder can be observed.

■ ASSOCIATED CONTENT

Supporting Information

The Supporting Information is available free of charge at https://pubs.acs.org/doi/10.1021/acsami.0c17192.

Uniaxial tensile tests of 10PLA-MNC and after 4 months degradation; printed 10PLA-MNC specimens before and after tensile/three-point bending tests; fracture surface morphologies of 10PLA-MNC tensile specimens; Uniaxial tensile deformation sequences of 2D hex77, 2D hex66, and 2D hex55 soft networks (PDF)

Movie S1 − Deformation behavior of soft network with hex88 microstructure (MP4)

Movie S2 − 4D transformation process of double-layer LAAO (MP4)

■ AUTHOR INFORMATION

Corresponding Authors

Liwu Liu − *Department of Astronautical Science and Mechanics, Harbin Institute of Technology (HIT), Harbin 150001, China*; Email: liulw@hit.edu.cn

Jinsong Leng − *Center for Composite Materials and Structures, Harbin Institute of Technology (HIT), Harbin 150080, China*; orcid.org/0000-0001-5098-9871; Email: lengjs@hit.edu.cn

Authors

Cheng Lin − *Department of Astronautical Science and Mechanics, Harbin Institute of Technology (HIT), Harbin 150001, China*

Yanju Liu − *Department of Astronautical Science and Mechanics, Harbin Institute of Technology (HIT), Harbin 150001, China*

Complete contact information is available at: https://pubs.acs.org/10.1021/acsami.0c17192

Notes

The authors declare no competing financial interest.

■ ACKNOWLEDGMENTS

The authors gratefully acknowledge the financial supports provided by the National Natural Science Foundation of China (Grant Nos. 11632005 and 11672086). The authors also thank Xiaozhou Xin for his kind help.

■ ABBREVIATIONS

LAAO, left atrial appendage occluder; LAA, left atrial appendage; SMP, shape memory polymer; AF, atrial fibrillation; OACs, oral anticoagulants; FEA, finite element analysis; MNCs, magnetic nanocomposites; FDM, fused deposition modeling; SEM, scanning electron microscope; H&E, hematoxylin−eosin

■ REFERENCES

(1) Pan, S.; Yin, J.; Yu, L.; Zhang, C.; Zhu, Y.; Gao, Y.; Chen, Y. 2D MXene-Integrated 3D-Printing Scaffolds for Augmented Osteosarco-

ma Phototherapy and Accelerated Tissue Reconstruction. *Adv. Sci. (Weinh)* **2020**, *7*, 1901511.
(2) Goyanes, A.; Det-Amornrat, U.; Wang, J.; Basit, A. W.; Gaisford, S. 3D Scanning and 3D Printing as Innovative Technologies for Fabricating Personalized Topical Drug Delivery Systems. *J. Controlled Release* **2016**, *234*, 41−48.
(3) Zhou, F.; Hong, Y.; Liang, R.; Zhang, X.; Liao, Y.; Jiang, D.; Zhang, J.; Sheng, Z.; Xie, C.; Peng, Z.; Zhuang, X.; Bunpetch, V.; Zou, Y.; Huang, W.; Zhang, Q.; Alakpa, E. V.; Zhang, S.; Ouyang, H. Rapid Printing of Bio-inspired 3D Tissue Constructs for Skin Regeneration. *Biomaterials* **2020**, *258*, 120287.
(4) Xin, X.; Liu, L.; Liu, Y.; Leng, J. 4D Printing Auxetic Metamaterials with Tunable, Programmable, and Reconfigurable Mechanical Properties. *Adv. Funct. Mater.* **2020**, *30*, 2004226.
(5) Zhao, Q.; Qi, H. J.; Xie, T. Recent Progress in Shape Memory Polymer: New Behavior, Enabling Materials, and Mechanistic Understanding. *Prog. Polym. Sci.* **2015**, *49*−*50*, 79−120.
(6) Xin, X.; Liu, L.; Liu, Y.; Leng, J. Origami-inspired Self-deployment 4D Printed Honeycomb Sandwich Structure with Large Shape Transformation. *Smart Mater. Struct.* **2020**, *29*, 65015.
(7) Xie, R.; Hu, J.; Hoffmann, O.; Zhang, Y.; Ng, F.; Qin, T.; Guo, X. Self-fitting Shape Memory Polymer Foam Inducing Bone Regeneration: A Rabbit Femoral Defect Study. *Biochim. Biophys. Acta, Gen. Subj.* **2018**, *1862*, 936−945.
(8) Peterson, G. I.; Dobrynin, A. V.; Becker, M. L. Biodegradable Shape Memory Polymers in Medicine. *Adv. Healthcare Mater.* **2017**, *6*, 1700694.
(9) Zhao, W.; Liu, L.; Zhang, F.; Leng, J.; Liu, Y. Shape Memory Polymers and Their Composites in Biomedical Applications. *Mater. Sci. Eng., C* **2019**, *97*, 864−883.
(10) Lin, C.; Liu, L.; Liu, Y.; Leng, J. The compatibility of polylactic acid and polybutylene succinate blends by molecular and mesoscopic dynamics. *Int. J. Smart Nano Mater.* **2020**, *11*, 24−37.
(11) Zhao, Q.; Wang, J.; Cui, H.; Chen, H.; Wang, Y.; Du, X. Programmed Shape-Morphing Scaffolds Enabling Facile 3D Endothelialization. *Adv. Funct. Mater.* **2018**, *28*, 1801027.
(12) Lin, C.; Zhang, L.; Liu, Y.; Liu, L.; Leng, J. 4D Printing of Personalized Shape Memory Polymer Vascular Stents with Negative Poisson's Ratio Structure: A Preliminary Study. *Sci. China: Technol. Sci.* **2020**, *63*, 578−588.
(13) Falahati, M.; Ahmadvand, P.; Safaee, S.; Chang, Y.; Lyu, Z.; Chen, R.; Li, L.; Lin, Y. Smart Polymers and Nanocomposites for 3D and 4D Printing. *Mater. Today* **2020**, *40*, 215.
(14) Zhao, W.; Zhang, F.; Leng, J.; Liu, Y. Personalized 4D printing of Bioinspired Tracheal Scaffold Concept based on Magnetic Stimulated Shape Memory Composites. *Compos. Sci. Technol.* **2019**, *184*, 107866.
(15) Wolf, P. A.; Abbott, R. D.; Kannel, W. B. Atrial Fibrillation as an Independent Risk Factor for Stroke: the Framingham Study. *Stroke* **1991**, *22*, 983−988.
(16) Huang, H.; Liu, Y.; Xu, Y.; Wang, Z.; Li, Y.; Cao, K.; Zhang, S.; Yang, Y.; Yang, X.; Huang, D.; Yu, B.; Su, X.; Wu, L.; Huang, C. Percutaneous Left Atrial Appendage Closure with the LAmbre Device for Stroke Prevention in Atrial Fibrillation: A Prospective, Multicenter Clinical Study. *JACC: Cardiovascular Interventions* **2017**, *10*, 2188−2194.
(17) Ostermayer, S. H.; Reisman, M.; Kramer, P. H.; Matthews, R. V.; Gray, W. A.; Block, P. C.; Omran, H.; Bartorelli, A. L.; Della Bella, P.; Di Mario, C.; Pappone, C.; Casale, P. N.; Moses, J. W.; Poppas, A.; Williams, D. O.; Meier, B.; Skanes, A.; Teirstein, P. S.; Lesh, M. D.; Nakai, T.; Bayard, Y.; Billinger, K.; Trepels, T.; Krumsdorf, U.; Sievert, H. Percutaneous Left Atrial Appendage Transcatheter Occlusion (PLAATO System) to Prevent Stroke in High-Risk Patients with Nonrheumatic Atrial Fibrillation - Results from the International Multicenter Feasibility Trials. *J. Am. Coll. Cardiol.* **2005**, *46*, 9−14.
(18) Wolf, P. A.; Abbott, R. D.; Kannel, W. B. Atrial Fibrillation as an Independent Risk Factor for Stroke: the Framingham Study. *Stroke* **1991**, *22*, 983−988.
(19) Petersen, P.; Godtfredsen, J.; Boysen, G.; Andersen, E.; Andersen, B. Placebo-controlled, Randomised Trial of Warfarin and Aspirin for Prevention of Thromboembolic Complications in Chronic Atrial Fibrillation: The Copenhagen AFASAK Study. *Lancet* **1989**, *333*, 175−179.
(20) Kakkar, A. K.; Mueller, I.; Bassand, J. P.; Fitzmaurice, D. A.; Goldhaber, S. Z.; Goto, S.; Haas, S.; Hacke, W.; Lip, G. Y.; Mantovani, L. G.; Turpie, A. G. G.; Van Eickels, M.; Misselwitz, F.; Rushton-Smith, S.; Kayani, G.; Wilkinson, P.; Verheugt, F. W. A. For the Garfield Registry Investigators. Risk Profiles and Antithrombotic Treatment of Patients Newly Diagnosed with Atrial Fibrillation at Risk of Stroke: Perspectives from the International, Observational, Prospective GARFIELD Registry. *PLoS One* **2013**, *8*, e63479.
(21) Belgaid, D. R.; Khan, Z.; Zaidi, M.; Hobbs, A. Prospective Randomized Evaluation of the Watchman Left Atrial Appendage Closure Device in Patients with Atrial Fibrillation versus Long-term Warfarin Therapy the PREVAIL Trial. *Int. J. Cardiol.* **2016**, *219*, 177−179.
(22) Saw, J. Editorial Commentary: Percutaneous Left Atrial Appendage Closure for Stroke Prevention. *Trends Cardiovasc. Med.* **2016**, *26*, 200−201.
(23) Amin, Z.; Hijazi, Z. M.; Bass, J. L.; Cheatham, J. P.; Hellenbrand, W. E.; Kleinman, C. S. Erosion of Amplatzer Septal Occluder Device after Closure of Secundum Atrial Septal Defects: Review of Registry of Complications and Recommendations to Minimize Future Risk. *Catheter. Cardio. Inte.* **2004**, *63*, 496−502.
(24) Wertman, B.; Azarbal, B.; Riedl, M.; Tobis, J. Adverse Events Associated with Nickel Allergy in Patients Undergoing Percutaneous Atrial Septal Defect or Patent Foramen Ovale Closure. *J. Am. Coll. Cardiol.* **2006**, *47*, 1226−1227.
(25) Liu, S.; Peng, K.; Hsiao, C.; Liu, K.; Chung, H.; Chen, J. Novel Biodegradable Polycaprolactone Occlusion Device Combining Nanofibrous PLGA/Collagen Membrane for Closure of Atrial Septal Defect (ASD). *Ann. Biomed. Eng.* **2011**, *39*, 2759−2766.
(26) Sideris, E.; Toumanides, S.; Agricola, T.; Moulopoulos, S. Abstract 11766: Long Term Follow-up and Outcome of Atrial Fibrillation Patients with Left Atrial Appendage Obliteration Using Wireless Absorbable Occluders. *Circulation* **2016**, *134*, A11766.
(27) Toumanides, S.; Sideris, E. B.; Agricola, T.; Moulopoulos, S. Transcatheter Patch Occlusion of the Left Atrial Appendage Using Surgical Adhesives in High-Risk Patients with Atrial Fibrillation. *J. Am. Coll. Cardiol.* **2011**, *58*, 2236−2240.
(28) Liu, J.; Zhang, Y. Soft Network Materials with Isotropic Negative Poisson's Ratios over Large Strains. *Soft Matter* **2018**, *14*, 693−703.
(29) Ma, Q.; Cheng, H.; Jang, K.; Luan, H.; Hwang, K.; Rogers, J. A.; Huang, Y.; Zhang, Y. A Nonlinear Mechanics Model of Bio-inspired Hierarchical Lattice Materials Consisting of Horseshoe Microstructures. *J. Mech. Phys. Solids* **2016**, *90*, 179−202.
(30) Ma, Y.; Feng, X.; Rogers, J. A.; Huang, Y.; Zhang, Y. Design and Application of 'J-shaped' Stress-strain Behavior in Stretchable Electronics: a review. *Lab Chip* **2017**, *17*, 1689−1704.
(31) Jang, K. I.; Chung, H. U.; Xu, S.; Lee, C. H.; Luan, H.; Jeong, J.; Cheng, H.; Kim, G. T.; Han, S. Y.; Lee, J. W.; Kim, J.; Cho, M.; Miao, F.; Yang, Y.; Jung, H. N.; Flavin, M.; Liu, H.; Kong, G. W.; Yu, K. J.; Rhee, S. I.; Chung, J.; Kim, B.; Kwak, J. W.; Yun, M. H.; Kim, J. Y.; Song, Y. M.; Paik, U.; Zhang, Y.; Huang, Y.; Rogers, J. A. Soft Network Composite Materials with Deterministic and Bio-Inspired Designs. *Nat. Commun.* **2015**, *6*, 6566.
(32) Liu, J.; Zhang, Y. A Mechanics Model of Soft Network Materials with Periodic Lattices of Arbitrarily Shaped Filamentary Microstructures for Tunable Poisson's Ratios. *J. Appl. Mech.* **2018**, *85*, 1 DOI: 10.1115/1.4039374.
(33) Chacón, J. M.; Caminero, M. A.; García-Plaza, E.; Núñez, P. J. Additive Manufacturing of PLA Structures using Fused Deposition Modelling: Effect of Process Parameters on Mechanical Properties and Their Optimal Selection. *Mater. Des.* **2017**, *124*, 143−157.
(34) Farah, S.; Anderson, D. G.; Langer, R. Physical and Mechanical Properties of PLA, and their Functions in Widespread Applications - a comprehensive review. *Adv. Drug Delivery Rev.* **2016**, *107*, 367−392.
(35) Göpferich, A. Mechanisms of Polymer Degradation and Erosion. *Biomaterials* **1996**, *17*, 103−114.

(36) Jiang, L.; Zhang, J.; Wolcott, M. P. Comparison of Polylactide/Nano-sized Calcium Carbonate and Polylactide/Montmorillonite Composites: Reinforcing Effects and Toughening Mechanisms. *Polymer* **2007**, *48*, 7632−7644.
(37) Yang, W.; Sherman, V. R.; Gludovatz, B.; Schaible, E.; Stewart, P.; Ritchie, R. O.; Meyers, M. A. Lawrence Berkeley National Lab. LBNL, B. C. U. S. On the Tear Resistance of Skin. *Nat. Commun.* **2015**, *6*, 6649.
(38) Shi, D.; Kang, Y.; Zhang, G.; Gao, C.; Lu, W.; Zou, H.; Jiang, H. Biodegradable Atrial Septal Defect Occluders: A current review. *Acta Biomater.* **2019**, *96*, 68−80.
(39) Huang, Y.; Kong, J. F.; Venkatraman, S. S. Biomaterials and Design in Occlusion Devices for Cardiac Defects: A review. *Acta Biomater.* **2014**, *10*, 1088−1101.
(40) Lu, W.; Ouyang, W.; Wang, S.; Liu, Y.; Zhang, F.; Wang, W.; Pan, X. A Novel Totally Biodegradable Device for Effective Atrial Septal Defect Closure: A 2-year Study in Sheep. *J. Interv. Cardiol.* **2018**, *31*, 841−848.
(41) Xie, Z. F.; Wang, S. S.; Zhang, Z. W.; Zhuang, J.; Liu, X. D.; Chen, X. M.; Zhang, G.; Zhang, D. A Novel-Design Poly-L-Lactic Acid Biodegradable Device for Closure of Atrial Septal Defect: Long-Term Results in Swine. *Cardiology* **2016**, *135*, 179−187.
(42) Ramot, Y.; Haim-Zada, M.; Domb, A. J.; Nyska, A. Biocompatibility and Safety of PLA and its Copolymers. *Adv. Drug Delivery Rev.* **2016**, *107*, 153−162.
(43) Li, X.; Kong, X.; Zhang, Z.; Nan, K.; Li, L.; Wang, X.; Chen, H. Cytotoxicity and Biocompatibility Evaluation of N,O-carboxymethyl Chitosan/Oxidized Alginate Hydrogel for Drug Delivery Application. *Int. J. Biol. Macromol.* **2012**, *50*, 1299−1305.
(44) Kim, Y.; Yuk, H.; Zhao, R.; Chester, S. A.; Zhao, X. Printing Ferromagnetic Domains for Untethered Fast-transforming Soft Materials. *Nature* **2018**, *558*, 274−279.
(45) Madani, S. Z. M.; Reisch, A.; Roxbury, D.; Kennedy, S. M. A Magnetically Responsive Hydrogel System for Controlling the Timing of Bone Progenitor Recruitment and Differentiation Factor Deliveries. *ACS Biomater. Sci. Eng.* **2020**, *6*, 1522−1534.
(46) Cezar, C. A.; Kennedy, S. M.; Mehta, M.; Weaver, J. C.; Gu, L.; Vandenburgh, H.; Mooney, D. J. Biphasic Ferrogels for Triggered Drug and Cell Delivery. *Adv. Healthcare Mater.* **2014**, *3*, 1869−1876.
(47) Ramot, Y.; Haim-Zada, M.; Domb, A. J.; Nyska, A. Biocompatibility and Safety of PLA and its Copolymers. *Adv. Drug Delivery Rev.* **2016**, *107*, 153−162.
(48) Bos, R. R.; Rozema, F. R.; Boering, G.; Nijenhuis, A. J.; Pennings, A. J.; Verwey, A. B.; Nieuwenhuis, P.; Jansen, H. W. Degradation of and Tissue Reaction to Biodegradable Poly(L-lactide) for use as Internal Fixation of Fractures: a Study in Rats. *Biomaterials* **1991**, *12*, 32−36.
(49) Zhang, D.; Wei, Y.; Chen, K.; Zhang, X.; Xu, X.; Shi, Q.; Han, S.; Chen, X.; Gong, H.; Li, X.; Zhang, J. Biocompatible Reactive Oxygen species (ROS)-responsive Nanoparticles as Superior Drug Delivery Vehicles. *Adv. Healthcare Mater.* **2015**, *4*, 69−76.
(50) Zhao, Q.; Wang, J.; Wang, Y.; Cui, H.; Du, X. A Stage-specific Cell-manipulation Platform for Inducing Endothelialization on Demand. *National Science Review* **2020**, *7*, 629−643.
(51) Zhao, Q.; Li, C.; Shum, H. C.; Du, X. Shape-adaptable Biodevices for Wearable and Implantable Applications. *Lab Chip* **2020**, *20*, 4321.
(52) Zhang, F.; Wang, L.; Zheng, Z.; Liu, Y.; Leng, J. Magnetic Programming of 4D printed Shape Memory Composite Structures. *Composites, Part A* **2019**, *125*, 105571.
(53) Earley, M. J. How to Perform a Transseptal Puncture. *Heart* **2008**, *95*, 85−92.

https://dx.doi.org/10.1021/acsami.0c17192
ACS Appl. Mater. Interfaces 2021, 13, 12668−12678